The 9th European Congress on Computational Methods in Applied Sciences and Engineering
ECCOMAS Congress 2024
3 – 7 June 2024, Lisboa, Portugal

MODELING OF 3D-PRINTED SOFT PNEUMATIC ACTUATORS

F.BUONAMICI[†*], L.PUGGELLI[*], L.GOVERNI[*], Y.VOLPE[*], L.TORZINI[*]

[*] Department of Industrial Engineering of Florence, via di S. Marta 3, 50139, Florence - Italy
[†]Corresponding author francesco.buonamici@unifi.it

Keywords: Soft Actuator, Pneumatic Actuator, 3D printing, Modeling, Soft Material
Summary. Soft Pneumatic Actuators (SPAs) have a simple structure of inner chambers that can be deformed to generate force when pressurized. Additive Manufacturing (AM) has been used to enhance SPAs by leveraging design freedom and customization for specific tasks. This study aims to develop a Finite Element Method (FEM) model to simulate a generic 3D-printed bellow SPA performing planar bending motion under pressure. The model, which can be used with different SPA design parameters, evaluates properties such as bending angle and exerted forces. The performance of a bellow SPA is influenced by factors such as its main dimensions, material, operating pressure, and chamber shape. This study considered three main contributors to bending behavior: wall chamber thickness, the number of bellow segments, and operating pressure. Various configurations were 3D-printed in Thermoplastic Polyurethane (TPU) and tested using a physical rig. FEM analyses were conducted within Ansys 2019 using static structural analysis. The second-order Ogden model was chosen for the hyper-elastic material according to reference [1]. Material parameters were identified for limited configurations through an optimization process that minimized the bending angle error. Other actuator configurations were simulated using various sets of parameters and compared with physical test results. The results showed a valid approximation across different actuator configurations. This study has developed an effective methodology to simulate the behavior of a generic 3D-printed TPU bellow SPA with a satisfactory level of approximation.

1 INTRODUCTION

Soft robots are a subcategory of robots, known for their high compliance, enabling them to function in various environments [2] and adapt their shape to different scenarios. This is especially beneficial in human-robot interactions [3]. This work focuses on Fluidic Elastomer Actuators (FEAs), a type of actuation system that operates using pressurized fluids, specifically Soft Pneumatic Actuators (SPAs) that use pressurized air. SPAs have a simple structure of interconnected chambers that expand and deform under pressure. The type of action, such as bending, twisting, or extending, can be programmed based on the actuator's morphology, as illustrated in Fig 1.

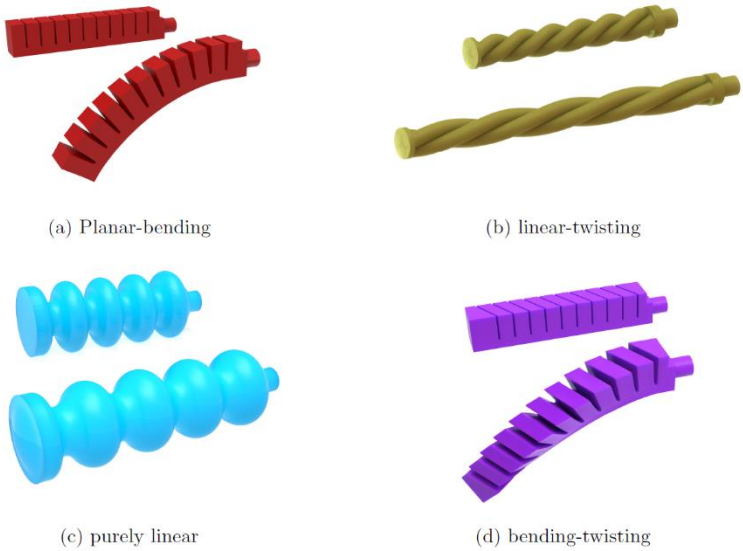

Figure 1: Classification of pneumatic bellow-type actuators based on the kind of movement they produce under pressure. The actuator's resting and pressured states are shown in picture [4].

The model proposed by Mosadeg et al. [5], used in this work, falls under the "Planar Bending" category. This model generates an expansion of the chambers under increased pressure, leading to contact between them and resulting in a pure bending of the entire actuator in the plane. The actuator's response to applied pressure depends on both the materials used and the actuator's geometry. The bending performance is directly influenced by these factors, making geometrical and material parameters critical design parameters. The influence of geometrical parameters such as gap size between two consecutive bellows, wall thickness, bottom layer thickness, chamber width, number of chambers, and the type of cross on the bending angle of SPAs was studied [6-9]. There are two methods to characterize actuator responses. The first involves creating and testing numerous specimens for full factorial analysis, which provides an understanding of a specific actuator's behavior under certain conditions. However, this method requires significant time and resources, and tests must be repeated if conditions or the actuator change. The alternative method uses Finite Element Method (FEM) simulations. Once boundary conditions are identified, these simulations can replicate a specific component's behavior, making this approach more efficient as it avoids physical testing and adapts easily to changes. However, predicting the behavior of soft actuators can be challenging due to their inherent flexibility and non-linear behavior. SPAs display complex deformation under pressure due to the component's geometry and the hyperelastic and anisotropic behaviors of the material. FEM modeling allows engineers to simulate these deformations, providing insights into the actuator's motion range, force output, and deformation. [10,11]. Designing SPAs to meet application requirements is critical. FE analysis can significantly benefit soft systems:

• With given geometrical properties and load case, actuator behavior can be predicted.
• Performance can be evaluated and optimal actuator geometry can be chosen to meet design specifications [12], saving time and resources.

• Once optimal design is found, simulation settings can be adjusted to match real behavior, especially useful for highly elastic materials influenced by variables like humidity, temperature, load types, etc.

A key challenge in simulations is accurately replicating material behavior. Despite numerous models describing materials' hyper-elastic behavior [13-15], manufacturing process and specimen geometric characteristics can complicate modeling.

This study developed a FEM model to simulate the behavior of TPU soft pneumatic actuators made using Fused Filament Fabrication (FFF) 3D printing. The study evaluated the influence of three parameters: the number of bellows (N), the bellow wall thickness (S), and the operating pressure (P) on the bending angle (α) and the extreme force exerted (F). The behavior was studied for wall thicknesses of 1.6, 2, and 2.4 mm, pressures of 1, 2, and 3 bar, and the number of bellows chosen were 9, 11, and 13, resulting in 27 possible combinations. Tests were conducted on real actuators with different configurations. A FEM model was created, two hyperelastic material models and three material parameters were tested, the error was evaluated, and the material parameters that best fit the practical results were derived through an optimization process. The study aims to create an SPA model that can predict a real actuator's behavior under known working conditions.

2 MATERIALS AND METHODS

2.1 Design and modeling

Soft robotics' motion path is typically programmed into the actuator design, making the ability to design and model soft actuators crucial. Soft actuators were modeled in 3D CAD environments using SolidWorks 2022 (Dassault Systèmes). The design was optimized for FFF 3D printing to avoid supports. Besides the three parameters studied, cross-section choice significantly affects mechanical behavior. Literature [9] found rectangular cross-sections superior in terms of bending and force exertion at the same air pressure, hence only rectangular cross-sections were considered. Given their frequent use in rehabilitation applications like wearable devices, the SPA's size and shape mimic an average human finger. As shown in Fig.2, the actuator's overall length is 115 mm, height 20 mm, and width 17 mm.

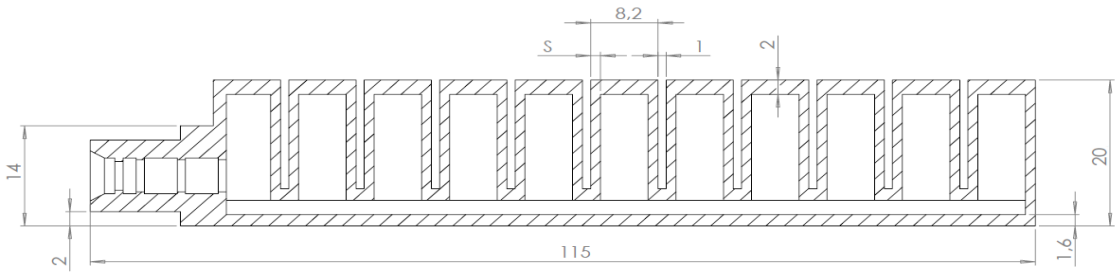

Figure 2: Section view of the bellow finger with N = 11 bellows

Afterward, the CAD models are imported to the ANSYS Workbench 2019 r3 (ANSYS Inc.) along with the material model developed to simulate the soft actuators to predict their behavior and optimize their performance.

2.2 Fabrication

SPAs were manufactured using an FDM 3D printer (Original Prusa i3 MK3+ [16]) without supports, limiting post-processing. This was possible by printing the actuators sideways, eliminating internal supports, and leaving only the actuator's upper part overhanging. Previous tests by authors showed this orientation reduces air leakage risk. A commercial TPU, NinjaFlex [17], with a shore hardness of 85, was used for 3D printing the soft actuators. PrusaSlicer V2.5.0 was used for reading the STL file.

2.3 Experimental setup

The pressurized air is supplied by a portable compressor (Hyundai™ KWU750-24L). Airflow control is done through a pressure gauge regulator at the compressor outlet; the pressure range used in the experiment is 1-3 bar. An electrical circuit was created based on Arduino® Uno board (Arduino AG, Chiasso CH), to allow the opening and closing of two solenoid valves through which pressurized air can enter and exit. Actuators were fixed horizontally using a 3D-printed PLA support and pressurized air is fed into actuators via a 5 mm PVC pipe. A CCD Mono 480p camera (IDS UI 2310 M) was used to capture images of the actuator under pressure, to take measurements on the images. To measure the force exerted at the tip of the pressurized actuators, a digital scale with a sensitivity of 0.1 g was used. The actuator was then fixed at one end and the other one was placed 5 mm above the scale's plate, allowing it to flex and exert a force on a 3D-printed square once pressurized.

3 MECHANICAL BEHAVIOR

Considering all possible combinations of P, N, and S, 27 specimens have been tested. For what concerns the optimization process, only 9 specific specimens are required to estimate the main effects of the 3 factors (see Tab. 1).

3.1 Bending behavior

To assess whether the FEM models were able to predict the behavior of the real models, the bending angle α, seen in Fig. 3, was measured at the maximum deflection.

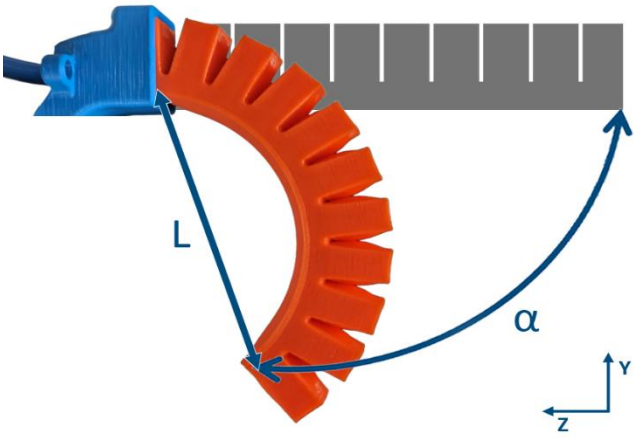

Figure 3: 3D printed actuator pressurized and corresponding bending angle.

The measurement was performed on the captured image using a specifically devised routine coded in MATLAB®. By knowing the bending angle (α) and the length of the cord (L), which was calculated using the height of the PLA support as a reference, were calculated the ΔZ and ΔY values of the actuator tip relative to the horizontal position. The test was conducted with variations in the three parameters mentioned above, resulting in 27 unique combinations. For each of these combinations, the test was performed on three identical specimens. Each specimen was tested three times, yielding a total of 243 images. Once all the images had been obtained and processed, the average values were calculated. Tab 1 shows only the 9 combinations used as the main reference for the FEM analysis and optimization process.

Table 1: Main experimental actuator tip displacements used as reference for FEA process

	N	**S [mm]**	**P [bar]**	**Actual Displacement [mm]**	
				Δ*Z*	**ΔY**
#1	9	1,6	1	9,4	9
#2	9	2	2	23,9	9
#3	9	2,4	3	19,8	9
#4	11	1,6	1	17,9	11
#5	11	2	2	27,3	11
#6	11	2,4	3	30,4	11
#7	13	1,6	1	16,3	13
#8	13	2	2	24,7	13
#9	13	2,4	3	23,0	13

3.2 Blocked Force behavior

The blocked force, a key performance metric for soft actuators, quantifies the force at the actuator's tip, reflecting efficiency in converting input pressure to output force. In tests, one end of the actuators is fixed, functioning like a cantilever beam, with the other end 5 mm above a digital scale. As input air pressure increases incrementally up to 3 bars, the output force also increases. This force measurement across the pressure range characterizes the actuator's force generation capabilities. The force value produced at each pressure level is recorded and converted to Newtons. The same 9 parameter combinations were tested on three actuators, with each test repeated thrice and values averaged. These averages are in Tab 2.

Table 2: Experimental forces exerted

N	**S [mm]**	**P [bar]**	**Force [N]**
9	1,6	1	0,76
9	2	2	1,54
9	2,4	3	1,43
11	1,6	1	0,76
11	2	2	1,79
11	2,4	3	1,95
13	1,6	1	1,03
13	2	2	1,82
13	2,4	3	1,74

4 FINITE ELEMENTS ANALYSIS

FE simulations were conducted using the "Static Structural Analysis" module in ANSYS Workbench 2019 R3 (ANSYS Inc.). The 3D CAD models of the soft actuators were directly imported into the ANSYS "Design Modeler". ANSYS was employed for the FE simulations of the soft actuators due to its capability of incorporating various hyperelastic material models, rendering it well-suited for static structural simulations involving hyperelastic materials.

4.1 Analysis settings

For the analysis setting, the “large deflection” option was used to best simulate the large deformations exhibited by the actuators during the application of internal pressure. Gradual load application was used to enhance simulation stability (from 0.1’’ to 1.0’’, 1e-4’’ time step). To replicate the test’s scenarios, “Fixed Support” was used at the actuator end to hold it in place while a positive pressure was applied all over the interior surfaces; the gravity force was considered for the simulations. Pressure was applied upon the internal surfaces of the actuators, using the desired value in a ramped form. “Frictionless contacts” were considered between the actuator bellow.

4.1.1 Bending simulations settings

Probes were added to measure displacements in the z-y plane in bending simulations. In addition, a ‘User Defined Function’ was used, by inputting a function as shown in eq (1):

$$((Ufz-UZ)^2 + (-Ufy-UY)^2)^(1/2) \quad (1)$$

Where *Ufz* and *Ufy* are respectively the displacement values of the tip of actuators measured in the real tests (and depend on the case at hand), with respect to the Z and Y axis. The values of *UZ* and *UY* are the actuator tip displacements obtained during simulations in the Z and Y axis, respectively. This function was used as an “objective function” for the optimization process, looking for that combination of material parameters that would bring the actuator to a configuration that would minimize the function.

4.1.2 Force simulations settings

A fixed flat plate was introduced into the model to simulate the digital scale plate, considering a “frictionless contact” between the actuator and the plate. A probe was introduced on the “fixed support” imposed on the plate, used to measure the force exerted by the actuator’s tip.

4.2 Meshing

Nonlinear Mechanical quadratic elements were used to mesh the CAD models of the soft actuators. The mesh used in all cases is suitable for hyper-elastic materials. An excessively fine mesh is not recommended since such materials can experience significant deformations [10]; initially, an element size of 1e-3 m was used. To further explore the possibility of adequately increasing and adapting the mesh to the pressurized actuator, a simulation was run using a mesh density of 1e-3 m and activating the ‘Nonlinear Adaptive Region’ option. Despite the

significantly longer runtime compared to a simulation without the 'Nonlinear Adaptive Region' option, it did not yield a significantly more accurate result. Therefore, it was decided not to use this option for subsequent runs. Finally, an element size of 1e-4 m was tested. Despite the increased time required and the presumed increase in accuracy, the difference was not significant enough to justify the increased computational cost of the simulation. For these reasons, a mesh with an element size of 1e-3 m was chosen.

4.3 Material models

Having an appropriate material model is crucial for a FEM simulation. TPU cannot be modeled by using a constant modulus of elasticity because rubber-like materials deformations are nonlinear and significantly large. Hyperelastic modeling, however, offers a solution to these issues. Among the large variety of hyperelastic models available, this study focuses on two of them, chosen based on suitability to TPU's structural properties and ease of modeling. Mooney–Rivlin 5 parameters model proposed by Tawk et al. [10] is an improvement from the Neo-Hookean model and it's typically depicted as a polynomial curve, ideal for representing rubbers and elastomers within a medium-to-large deformation range, defined as eq. (2):

$$W= C_{10} (I_1-3) +C_{01} (I_2-3) +C_{20} (I_1-3)^2+C_{11} (I_1-3) (I_2-3) +C_{02} (I_2-3)^2+1/D_1 (J-1)^2 \quad (2)$$

Where In are the invariants of deformation tensor, Cnn and D are the material parameters and J is the volumetric invariant of deformation tensor. The model was fitted to the experimental stress-strain data using the available curve fitting tools in ANSYS by the authors and the parameters are listed in Tab.3

Table 3: Material parameters obtained experimentally by Tawk et al. using the Mooney-Rivlin hyperelastic material model

Material Constant	Value [Unit]
C10	-0.233 [MPa]
C01	2.562 [MPa]
C20	0.116 [MPa]
C11	-0.561 [MPa]
C02	0.900 [MPa]
Incompressibility Parameter D1	0.000 [MPa^{-1}]

The elastic characteristics of printed NinjaFlex® TPU were also determined experimentally by Reppel et al. [1], who then fitted the experimental data onto a second-order Ogden model. Ogden model is a relatively simple, versatile constitutive model for various rubber-like materials, polymers, and even biological tissues [18]. For incompressible isotropic material under uniaxial stress, the Ogden hyperelastic model is defined as shown in eq. (3):

$$W(\lambda) = \sum^{N}_{(p=1)} 1\text{-}N\ \mu p/\alpha p\ (\lambda_1^{\alpha p} + \lambda_2^{\alpha p} - \lambda_3^{\alpha p})\text{-}\ 3 \quad (2)$$

where W is the strain energy density function, λ is the stretch, N is model order and μp and αp are material coefficients. In Reppel's work, two different sets of material parameters were obtained based on a uniaxial tension test made on unified DIN EN ISO 527-2 type 1BA specimens but different shell thicknesses; the two parameters set are listed in Tab.4.

Table 4: Material parameters derived experimentally by Reppel et al. using the Ogden hyperelastic material model

	$\mu 1$ [MPa]	$\alpha 1$ [MPa]	$\mu 2$ [MPa]	$\alpha 2$ [MPa]
Type 002	1,13	3,11	-13,17	-0,6
Type 005	0,13	3,05	-1214	-0,0054

4.3 FEM comparison

The first set of simulations was carried out to determine which material models, along with their respective parameters, most accurately replicated the outcomes of the actual tests. Were utilized the 9 combinations of actuators that were previously discussed and ran various simulations where the only variable was the material being simulated. To evaluate the similarity between the simulated model and the actual test, we calculated the Euclidean distance between the positions of the simulated actuator tip and the real actuator, using equation (1). Upon completion of the simulations, the calculated distance values were recorded in Tab. 5. Subsequently, we computed the mean and median values of these distances.

Table 5: Comparison of tip displacements using different combinations of models and material parameters against experimental values

N	**S [mm]**	**P [bar]**	**Actual Displacement [mm]**		**Error (distance) [mm]**		
			ΔZ	ΔY	Mooney-Rivlin (Tawk)	Ogden 002 (Reppel & Weinberg)	Ogden 005 (Reppel & Weinberg)
9	1,6	1	9,4	9	8,9	1,5	22,7
9	2	2	23,9	9	5,1	6,6	15,1
9	2,4	3	19,8	9	6,2	1,1	24,5
11	1,6	1	17,9	11	5,0	2,7	21,4
11	2	2	27,3	11	8,7	1,0	27,9
11	2,4	3	30,4	11	14,3	3,7	33,4
13	1,6	1	16,3	13	6,1	1,6	23,0
13	2	2	24,7	13	9,5	0,9	30,2
13	2,4	3	23,0	13	14,6	3,5	36,2
Mean Value					8,7	2,5	26,0
Median Value					8,7	1,6	24,5

5 OPTIMIZATION PROCESS

Looking at the results shown in Tab.5, it can be deduced that the second-order Ogen material model with the “002” specimens material parameters is the one that best replicates the real behavior of the actuators were printed and was therefore chosen as the reference material model from which to begin optimization. Despite the efforts, there remains a significant error between the experimental and simulated models. To address this, we chose to implement a ‘direct optimization’ process to minimize this difference. The optimization process was set up by

manually selecting Adaptive Single-Objective resolution method; for more details about this method, refer to the Ansys knowledge base [19]. Then an initial number of samples of 20 was chosen, with a maximum number of evaluations of 80, and a Convergence Tolerance of 1e-6 was set. Thus, starting from the material parameters of Ogden 002, the four material parameters (α1, μ1, α2, μ2) were set as input, applying a possible variation of 10%, and setting as the optimization objective function the minimization of eq. (1).

5.1 Results

After optimizing the 9 combinations of bellow number, wall thickness, and pressure, 9 sets of material parameters were obtained, each specific to a combination.

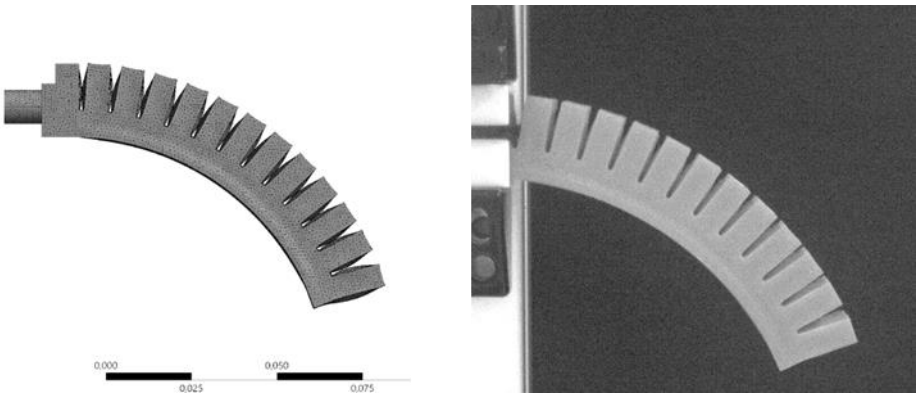

Figure 4: Comparison of the bending of the simulated model versus the real actuator

These parameters better describe the experimental data, showing excellent correspondence between simulated and real models (Fig.4). However, no specific parameter set was found to match actuators with similar characteristics (Fig. 5).

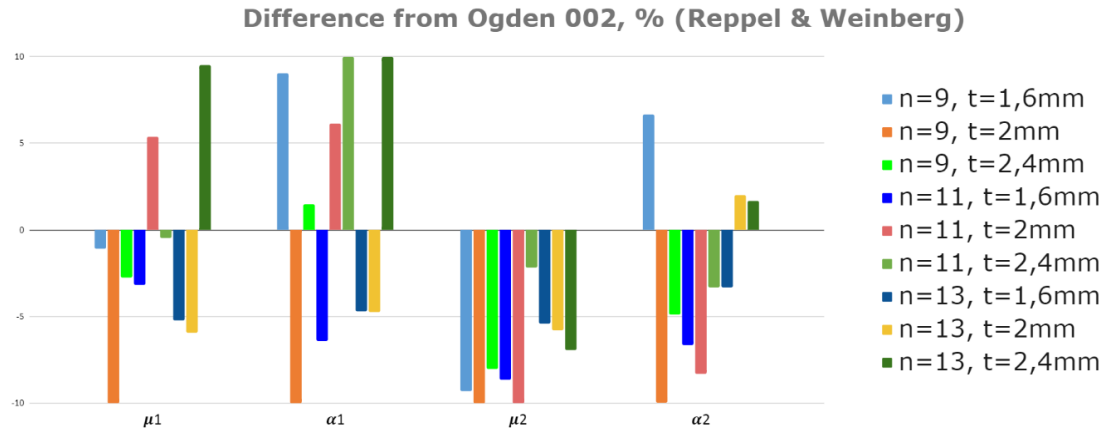

Figure 5: Variation of optimized material parameters compared with Ogden 002. Shades of blue - 1,6mm wall thickness; shades of red – 2mm wall thickness; shades of green – 2,4 mm wall thickness.

It was crucial to assess if the optimized parameters for a combination could accurately represent the same actuator under a different pressure. For this, 18 additional simulations were initiated using the optimized parameters but with different internal pressures. This process was replicated using 'Ogden 002' parameters. The distance between the simulated actuator tip and its real-life counterpart was recalculated, serving as the evaluation parameter. From Tab.6, using optimized parameters reduced the distance between the tips of simulated and real actuators globally by approximately 12% and 39%, respectively.

Table 6: Difference of tip displacement between experimental results and models simulated with Ogden 002 and optimized parameters used for the 9 main combinations

N	T (mm)	P (bar)	Ogden 002 (Reppel &Weinberg)	Optimized parameters
9	1,6	2	3,7	3,5
9	1,6	3	8	7,6
9	2	1	1,1	1,9
9	2	3	13,3	5,9
9	2,4	1	4,1	2,4
9	2,4	2	6,1	3,1
11	1,6	2	1,1	1,5
11	1,6	3	4,1	7,1
11	2	1	2,7	0,4
11	2	3	3,2	2,9
11	2,4	1	1,8	1,7
11	2,4	2	1,5	1,3
13	1,6	2	8,2	7,3
13	1,6	3	5,8	12,2
13	2	1	3,8	2,2
13	2	3	3,9	1,6
13	2,4	1	1,5	1,1
13	2,4	2	1,1	1,1
Mean Value			**4,1**	**3,6**
Median Value			**3,8**	**2,3**

Analyzing the results in Tab.6, errors were found concentrated at specific points in both material models. The simulated behavior of the actuators was also evaluated in terms of tip force and compared with actual results. Real test conditions were replicated in the FEM simulation, with actuators clamped at one end and positioned 5 mm above an immovable plane. A probe measured the force exerted at the desired pressure. The analysis setting was similar to previous simulations, using both material models, with results in Tab.7. After data collection, the error relative to the real actuator was calculated and averaged. It was observed that using optimized parameters didn't improve the prediction of forces exerted by the simulations over the reference ones.

Table 7 - Difference in exerted force between experimental results and models simulated with Ogden 002 and optimized parameters

N	S [mm]	P [bar]	Force (experimental) [N]	Ogden 002 (Reppel &Weinberg) [N]		Optimized parameters [N]	
				Force	Error	Force	Error
9	1,6	1	0,76	0,64	0,11	0,64	0,12
9	2	2	1,54	1,53	0,01	1,78	-0,24
9	2,4	3	1,43	2,17	-0,74	2,29	-0,86
11	1,6	1	0,76	0,75	0,00	0,82	-0,06
11	2	2	1,79	1,56	0,23	1,64	0,15
11	2,4	3	1,95	2,84	-0,89	2,86	-0,91
13	1,6	1	1,03	0,88	0,15	0,93	0,10
13	2	2	1,82	1,81	0,01	2,05	-0,23
13	2,4	3	1,74	2,53	-0,79	2,49	-0,75
Mean Value					**0,33**		**0,38**

8 CONCLUSION AND FUTURE WORKS

This study has successfully developed a methodology for accurately simulating the behavior of 3D printed Soft Pneumatic Actuators (SPAs). By focusing on key design parameters such as the number of bellows, wall thickness, and operating pressure, it effectively predicted the bending angle and exerted forces of the actuators. The use of the Ogden hyperelastic model and an optimization process to refine material parameters proved particularly valuable, resulting in a valid approximation across various actuator configurations. The findings have significant implications for the design and manufacturing of SPAs, providing insights into plausible material parameters for generic 3D printed bellow SPAs and facilitating the production of optimal actuators without the need for a trial-and-error approach. Future work will likely focus on further refining the simulation methodology and exploring additional parameters that may influence SPA performance. The goal is to enhance the capabilities of SPAs in soft robotics applications, thereby contributing to the advancement of this innovative field.

ACKNOWLEDGEMENT

This work is supported by the Spoke 9 within the Italian National Research Programme (NRP) TUSCANY HEALTH ECOSYSTEM (THE), CUP: B83C22003920001

REFERENCES

[1] Reppel, T. and Weinberg, K. 2019. “Experimental Determination of Elastic and Rupture Properties of Printed Ninjaflex”. Technische Mechanik - European Journal of Engineering Mechanics, 38(1). Doi: 10.24352/UB.OVGU-2018-010.

[2] Jaehwan, K., Jung, W.K., Hyun C.K., Lindong Z., Hyun-U K., and Ruth, M.M. 2019 “Review of soft actuator materials”. International Journal of Precision Engineering and Manufacturing, 20. Doi: 10.1007/s12541-019-00255-1

[3] Schmitt, F., Piccin, O., Barbè, L., and Bayle, B. 2018. “Soft robots manufacturing: A review” Frontiers in Robotics and AI, 5. Doi; 10.3389/frobt.2018.00084

[4] Torzini, L., Puggelli, L., Volpe, Y., Governi, L., and Buonamici, F. 2024. “Characterization of Fatigue Behavior of 3D Printed Pneumatic Fluidic Elastomer Actuators” Doi: 10.21203/rs.3.rs-4255722/v1

[5] Mosadegh, B., Panagiotis, P., Keplinger, C., Wennstedt, S., Shepherd, R.F., Gupta, U., Shim, J., Bertoldi, K., Walsh, C.J., and Whitesides, G.M. 2014. “Pneumatic networks for soft robotics that actuate rapidly”. Advanced Functional Materials, 24. DOI: 10.1002/adfm.201303288

[6] Stano, G., Arleo L., and Percoco G. 2020. “Additive Manufacturing for Soft Robotics: Design and Fabrication of Airtight, Monolithic Bending PneuNets with Embedded Air Connectors”. Micromachines 11(5). DOI: 10.3390/mi11050485

[7] Gao, R., Fang, J., Qiao, J., Li, C., and Zhang, L. 2022. “The bending control of the soft pneumatic finger”. Journal of Physics: Conference Series 2181(1). DOI: 10.1088/1742-6596/2181/1/012060

[8] Sun, Y., Zhang, Q., Chen, X., and Chen, H. 2019. “An Optimum Design Method of Pneu-Net Actuators for Trajectory Matching Utilizing a Bending Model and GA”. Mathematical Problems in Engineering. 10.1155/2019/6721897

[9] Hu, W., Mutlu, R., Li, W. and Alici, G. 2018. “A Structural Optimisation Method for a Soft Pneumatic Actuator”. Robotics 7(2). DOI: 10.3390/robotics7020024

[10] Tawk, C., Alici, G. 2020. “Finite Element Modeling in the Design Process of 3D Printed Pneumatic Soft Actuators and Sensors”. Robotics 9(3). DOI: 10.3390/robotics9030052

[11] Maruthavanan, D., Seibel, A., Schlattmann, J. 2021 “Fluid-Structure Interaction Modelling of a Soft Pneumatic Actuator”. Actuators, 10. DOI: 10.3390/act10070163

[12] Keong, B. A. W., Hua, R. Y. C. 2018. “A Novel Fold-Based Design Approach toward Printable Soft Robotics Using Flexible 3D Printing Materials”. Adv. Mater. Technol. 3(2). DOI: 10.1002/admt.201700172

[13] Xavier, M.S., Tawk, C.D., Fleming, A.J., Zolfagharian, A., Pinskier, J., Howard, D., Young, T., Lai, J., Harrison, S.M., Yong, Y.K.; Bodaghi, M. 2022. “Soft Pneumatic Actuators: A Review of Design, Fabrication, Modeling, Sensing, Control and Applications”. Institute of Electrical and Electronics Engineers (IEEE) 10. DOI: 10.1109/ACCESS.2022.3179589

[14] Batsuren, K., Yun, D. 2019. “Soft Robotic Gripper with Chambered Fingers for Performing In-Hand Manipulation”. Appl. Sci. 9. DOI: 10.3390/app9152967

[15]Steck, D., Qu, J., Kordmahale, S.B., Tscharnuter, D., Muliana, A. and Kameoka, J. 2018.” Mechanical responses of Ecoflex silicone rubber: Compressible and incompressible behaviors”. J. Appl. Polym. Sci., 136. DOI: 10.1002/app.47025

[16] Prusa: Prusa i3 M3KS+ (2024). https://www.prusa3d.com/category/original-prusa-i3-mk3s/ Accessed 19/06/2024

[17] NinjaTek: NinjaFlex 3D Printer Filament (2024). https://ninjatek.com/shop/ninjaflex/ Accessed 19/06/2024

[18] Ogden, R.W. 1972. “Large deformation isotropic elasticity–on the correlation of theory and experiment for incompressible rubberlike solids. Proc. R. Soc. London. A. Math. Phys 326. DOI: 10.1098/rspa.1972.0026.

[19] DesignXplorer User's Guide – CFD EXPERTS 2022. https://dl.cfdexperts.net/cfd_resources/Ansys_Documentation/DesignXplorer/DesignXplorer_Users_Guide.pdf Accessed 05/07/2024